ChemComm

COMMUNICATION

View Article Online
View Journal | View Issue

Cite this: *Chem. Commun.*, 2020, **56**, 12733

Received 2nd June 2020,
Accepted 11th September 2020

DOI: 10.1039/d0cc03876h

rsc.li/chemcomm

Fatty acids as biomimetic replication agents for luminescent metal–organic framework patterns†

Michael R. Hafner,[a] Francesco Carraro,[a] Lea A. Brandner,[a] Sivakumar Maniam,[b] Gianluca Grenci,[bc] Senka Ljubojevic-Holzer,[d] Helmut Bischof,[e] Roland Malli,[e] Sergey M. Borisov,[f] Christian Doonan *[g] and Paolo Falcaro *[ag]

Luminescent metal–organic frameworks (MOFs) are known to spontaneously self-assemble on human fingerprints. Here, we investigate the different chemical components of fingerprints and determine that MOF growth is predominantly induced by insoluble fatty acids. This finding shows that these simple biomolecules can be employed for the precise positioning of luminescent MOFs.

Spatially controlled self-assembly processes on substrates underpin MOF patterning protocols that are necessary for the fabrication of MOF-based devices (*e.g.* sensors).[1] Biomimetic replication is an emerging, bottom-up, water-based patterning strategy that capitalizes on the affinity of MOF precursors for certain biomolecules.[1,2] For example, proteins and carbohydrates that have a negative surface charge (isoelectric point, p. I. < 7)[3] are efficient heterogeneous nucleation agents for MOFs.[4,5] To this end, the water-soluble protein bovine serum albumin (BSA, p. I. = 5.3)[3] has been microcontact printed on silicon wafers and immersed in solutions containing MOF precursors to yield patterns of zeolitic imidazolate framework-8 (ZIF-8) and different luminescent MOFs (*i.e.*, $Ln_2(BDC)_3{*}(H_2O)_4$, BDC = 1,4-benzene dicarboxylic acid, Ln = lanthanide metal).[2] By assuming the presence of proteins and amino acids in fingerprint residues, biomimetic replication was tested on sebaceous secretions.[2,6,7] In minutes, MOF crystals could be selectively grown on fingerprint residues thus producing a fluorescent pattern (Fig. 1a and Fig. S1, ESI†). The potential of MOFs for forensic applications was investigated by Moret *et al.* and de Jong *et al.*[6,7] However, sebaceous secretions are composed of numerous molecular species that could potentially promote MOF formation and only a minor fraction is made of water-soluble proteins and amino acids (*vide infra*). Thus, we were motivated to systematically investigate which of the chemical species present in fingerprints engendered MOF crystallization. Our study revealed two significant findings relevant to both the application of MOFs to forensics and for applications that require precise positioning on substrates: (1) proteins do not contribute to the growth of $Tb_2(BDC)_3{*}(H_2O)_4$ MOFs on fingerprints, rather crystallisation is triggered by the fatty acid component (Fig. 1a); and (2) with respect to the biomimetic replication process, biomolecules with low solubility prevent the seeding of, uncontrolled, crystal growth in solution (Fig. 1b), which is crucial for the fabrication of MOF films and patterns.[1,2,4,8–13] Both aspects are demonstrated here for the first time. Chemical fingerprint analyses revealed that their composition is similar from person to person; however, the relative amount of the chemical components can vary depending on factors including age, gender, and habits.[14–19] Fingerprint residues on surfaces are typically a mixture of specific biomolecules including triglycerides, fatty acids (*e.g.* palmitic, oleic, and myristic acids), wax esters and squalene (Table 1).[16,20–22]

Proteins and amino acids are only minor components of the biomolecule mixture: the weight percentage (w%) in eccrine secretions ranges from 0.002% to 1%. The main amino acids in fingerprints have been identified as L-Serine, Glycine and L-Alanine and the protein content consists of a broad variety of mostly unknown macromolecules.[14,16,20–22] Given the assumption that the MOF growth was induced by this low amount of amino acids and proteins of unknown p. I. in sebaceous secretions and that the molecular components have not been investigated yet, here, we examine the crystallization of $Tb_2(BDC)_3{*}(H_2O)_4$, a green fluorescent MOF (for details on

[a] *Institute of Physical and Theoretical Chemistry, Graz University of Technology, Graz 8010, Austria. E-mail: paolo.falcaro@tugraz.at*
[b] *Mechanobiology Institute, National University of Singapore, 117411, Singapore*
[c] *Biomedical Engineering Department, National University of, Singapore, 117583, Singapore*
[d] *Department of Cardiology, Medical University of Graz, Graz 8036, Austria*
[e] *Gottfried Schatz Research Center, Molecular Biology and Biochemistry, Medical University of Graz, Graz 8010, Austria*
[f] *Institute of Analytical Chemistry and Food Chemistry, Graz University of Technology, Graz 8010, Austria*
[g] *Department of Chemistry, The University of Adelaide, Adelaide 5005, South Australia, Australia*

† Electronic supplementary information (ESI) available: Experimental details; XRD, FTIR, and optical, fluorescent and electron microscopy data. See DOI: 10.1039/d0cc03876h

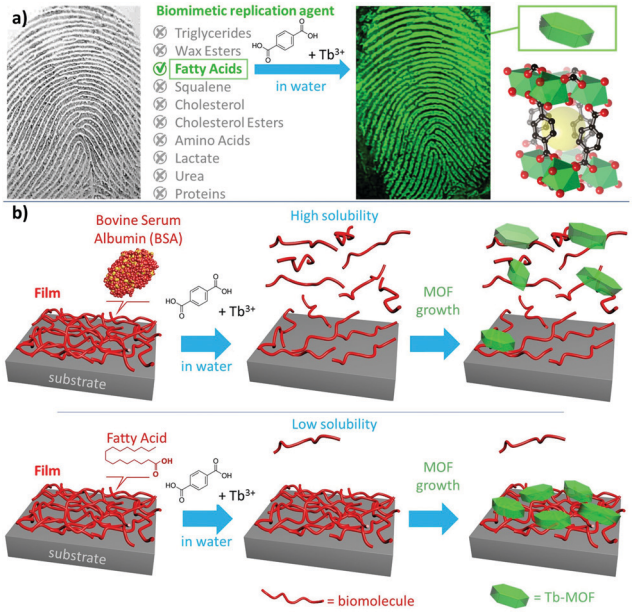

Fig. 1 (a) Human fingerprint and major biomolecules present in sebaceous and eccrine secretions. Tb-MOF can grow on fingerprints residues (see Fig. S1, ESI†). By investigating one biomolecule at the time, we found that fatty acids are the most effective biomimetic replication agents. (b) Film of biomolecules on a substrate and influence of its water solubility on the fabrication of a MOF film *via* biomimetic replication.

Table 1 Composition of fingerprint residue

Sebaceous secretion[16,22]		Eccrine secretion[16,20,22]	
Compound	Content [w%]	Compound	Content [w%]
Triglycerides	30–40	Amino Acids	0.002–0.02
Free fatty acids	15–25	Lactate	0.1–0.2
Wax esters	20–25	Urea	0.004–0.04
Squalene	10–12	Proteins	0.002–1
Cholesterol	1–3	Inorganics	0.02–0.6
Cholesterol esters	2–3	Water	98–99

absorption and emission of Tb-MOF, see Fig. S2, ESI†), on each of the main molecular components present in fingerprint residues.

We examined the molecular components of sebaceous and eccrine secretions (Table 1) along with BSA (the model protein previously used to simulate fingerprints)[2,8,11,23] as the biomimetic replication agent. For each class of molecule, we selected a representative compound: for triglycerides, trimyristin was selected;[16,19] for fatty acids, we selected palmitic acid;[15,16] for wax esters, we chose palmityl palmitate;[16,19] squalane was used instead of squalene due to its chemical stability towards oxidation;[16,19,24] and for amino acids, we selected L-serine.[16,25] Finally, cholesterol, lactate and urea were used as themselves. Each molecule was dissolved in water (2 mg mL^{-1}) and 2 μL drops of the respective solutions were cast on a glass slide. After drying, the samples were immersed for 30 s in a freshly prepared aqueous solution of MOF precursors (see ESI,† for details). Then, the substrates were washed with water and the glass slides were illuminated using a UV lamp (254 nm) to qualitatively verify the presence of the luminescent MOF.

Surprisingly, the fatty acid was the only sample that showed a homogenous luminescent spot (Fig. 2a and Fig. S3, ESI†), which is indicative of Tb-MOF growth *via* biomimetic replication. To observe the luminescent signal from drop-cast BSA solution, 30 mg mL^{-1} solution (15 times more concentrated than the fatty acid solution) was required. The MOF grown from BSA forms a luminescent ring (Fig. 2a and Fig. S3, ESI†). This inhomogeneity can be attributed to the Marangoni effect (*i.e.*, during the solvent evaporation the solvated molecule concentrates at the edge of the spot).[26] Thus the higher local concentration of BSA at the perimeter of the ring promotes biomimetic replication. On exposing the samples to longer reaction times (1 min, 5 min and 15 min), a qualitative increase in luminescence intensity under UV illumination was observed only in the case of the fatty acid spot (Fig. S3, ESI†). For BSA, the sharp ring that was initially observed appears to decompose over time (Fig. S3, ESI†). This may be caused by the high solubility of BSA in water,[2,27] as the protein would dissolve in solution and initiate the detachment of the MOF crystals grown on the BSA film. For other samples (*e.g.* wax and triglyceride), the increased luminescence from longer reaction time was qualitatively comparable to the background (uncoated SiO_2). Thus, the increase in luminescence intensity is likely due to the spontaneous formation of the Tb-MOF. It is noteworthy that without any seeding agents the Tb-MOF can be detected with the naked eye after 5 min. We quantitatively examined biomimetic replication as a function of the reaction time (1, 5 and 15 min), by measuring the optical response of the different films of biomolecules using a confocal fluorescence microscope (ESI,† for details, Fig. S15–S20). Intense luminescent signals with increasing intensity were measured only in the case of fatty acid and BSA (Fig. 2b and Fig. S15, S20, ESI†). The other biomolecules displayed only a few random luminescent spots after 5 minutes of reaction. The box-plot representation (Fig. 2b and Fig. S22, ESI†) shows the narrowest distribution of intensities and the most intense luminescence signal collected from the MOF grown on fatty acid films, suggesting the formation of a homogeneous MOF film. To investigate the formation of MOF crystals both on the substrate surface and in bulk solution, we monitored the luminescence intensity over time (15 minutes in total) using a camera. In each vial, a different biomolecule was deposited *via* drop-cast (see ESI,† for details) and dried to obtain a film. Then, the MOF precursor solution was added, and the formation of the luminescent material was detected only in the vial with the palmitic acid film (Fig. S21 and Video V1, ESI†). Optical and electron microscopy analyses were also performed to examine the growth of Tb-MOF on surfaces. The results are entirely consistent with previous observations and confirm that Tb-MOF grows homogeneously on fatty acids, that the concentrated ring of BSA decomposes with time and that the other biomolecules do not significantly promote MOF crystallization on surfaces (Fig. 2c–e and Fig. S4–S10, S23–S25, ESI†). In addition, complete dissolution of the biomacromolecule film was observed when water-soluble molecule films

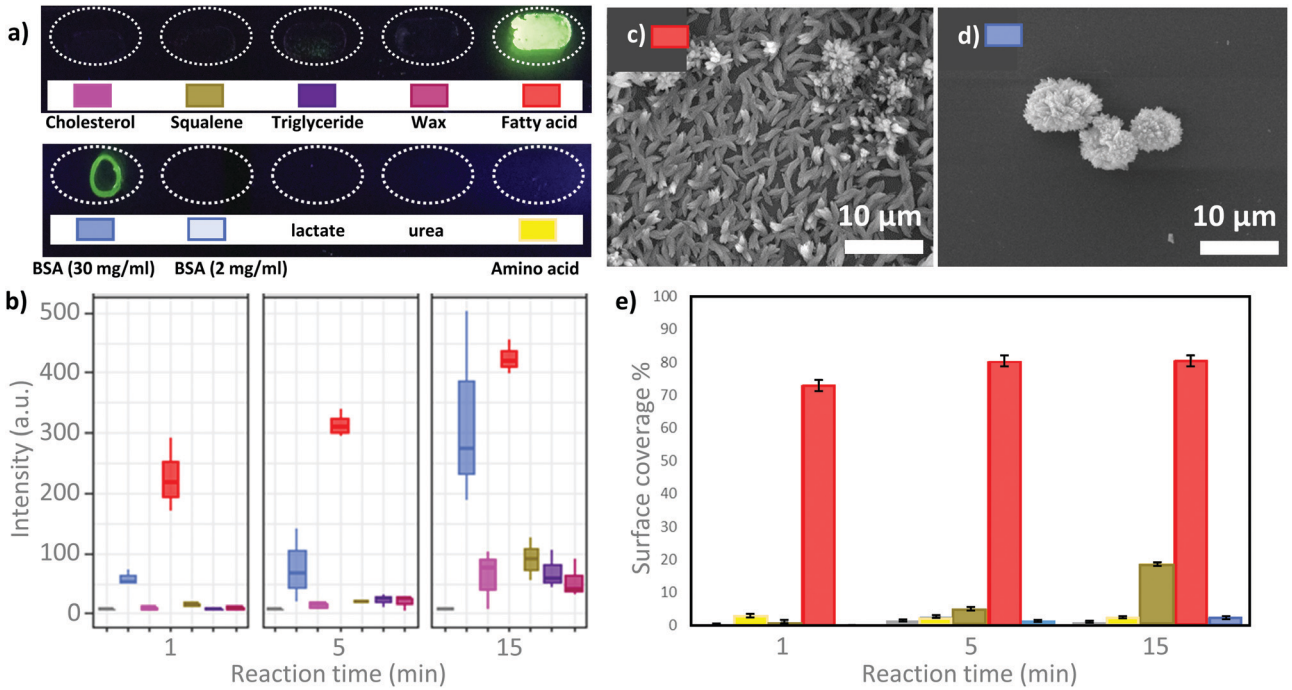

Fig. 2 (a) Glass slide with spots of biomolecules after 30 seconds of exposure to Tb-MOF precursors (upper row, f.l.t.r.: cholesterol, squalene, triglyceride, wax, fatty acid; lower row: f.l.t.r.: BSA (30 mg mL^{-1}), BSA, lactate, urea, amino acid). (b) Box-plot representation of luminescence intensity calculated from fluorescence micrographs (UV source: 340 nm, investigated area 250 by 150 µm; see Fig. S2, ESI,† for absorption and emission spectra) acquired at different MOF growth times for the different biomolecule spots (Fig. S15–S20, ESI†). For details about the interpretation of box-plots, see Fig. S22 (ESI†). (c) SEM micrograph of the Tb-MOF grown on drop-cast fatty acid (15 minutes of growth). (d) SEM micrograph of the Tb-MOF grown on drop-cast BSA (15 minutes of growth). (e) Growth-time dependent Tb-MOF surface coverage calculated from SEM micrographs (100× magnification, Fig. S23–S25, ESI†).

(*e.g.* BSA 2 mg mL^{-1}, urea, lactate and amino acid) were immersed in the MOF precursor solution.

Fourier-transform infrared spectroscopy (FT-IR) was used to evaluate the chemical composition of the biomolecule films after exposure to the MOF precursor solution. Close inspection of the data from the fatty acid (2 mg mL^{-1}) and BSA (30 mg mL^{-1}) films confirmed the presence of vibrational modes that could be assigned to Tb-MOF (*e.g.*, 1540 and 1400 cm^{-1}, de-protonated and coordinated 1,4-benzene dicarboxylic acid; 510 and 440 cm^{-1}, Tb–O stretching modes,[28,29] Fig. S11, ESI†). Furthermore, FT-IR confirmed that all the other molecules were ineffective biomimetic replication agents as vibrational modes of the Tb-MOF were not detected (Fig. S12 and S13, ESI†).

Next, XRD was performed to examine the crystallinity of the MOF films. The diffractograms of the control Tb-MOF (formed in solution without biomolecules), and the Tb-MOF on BSA were identical to those of previously reported Tb-MOF (Fig. S14, ESI†).[2,28–30] However, the XRD pattern of the Tb-MOF grown on a fatty acid substrate showed additional peaks (Fig. S14, ESI†): in addition to the (010) peak assigned to $Tb_2(BDC)_3{*}(H_2O)_4$, we measured peaks attributed to the crystallisation of the fatty acid molecules (4.9°, 7.4°, 12.3° and 17.3°)[31,32] and to the presence of Tb-palmitate (6°, 6.6°, 8° and 10°).[33] The absence of the Tb-MOF peaks at 11.3°, 14.6° and 15.6° indicates that the MOF crystals grown on fatty acids have a preferential direction of growth ((010)).[34] The morphology of these crystals, as determined using SEM, supports this hypothesis (Fig. 2c). The formation of Tb-palminate indicates a strong affinity between the fatty acid (carboxylic group) and the Tb cation.[3,4,35] Thus, we were motivated to explore the fabrication of microscopic MOF patterns from palmitic acid. A micropattern of palmitic acid was fabricated using micro-contact printing (µCP)[36,37] (see ESI,† for details, Fig. 3 and Fig. S24–S26), and the pattern was used for the controlled growth of Tb-MOF. This soft lithographic method allows for the facile preparation of complex patterns of fatty acids on several substrates including glass, silicon, polystyrene, and flexible polypropylene foils (Fig. 3 and Fig. S26–S28, ESI†). After exposing the patterned substrate to the MOF precursor solution, the MOF crystals were found to selectively grow on the fatty acid pattern (Fig. 3 and Fig. S27, ESI†).

In summary, we established that it is the presence of fatty acids that promotes the selective growth of luminescent MOF films on fingerprint residues. Indeed, fatty acids are significantly more efficient as biomimetic replication agents than BSA, a model protein used in previous studies. For example, after 1 minute of reaction, the drop-casting of a low concentration fatty acid solution (2 mg mL^{-1}, 20 µL) afforded a MOF film with a 300% more intense luminesce signal compared to that of the drop-cast high concentration BSA solution (30 mg mL^{-1}, 20 µL). Due to both the affinity of palmitic acid for cations and the low solubility in water of fatty acids, these

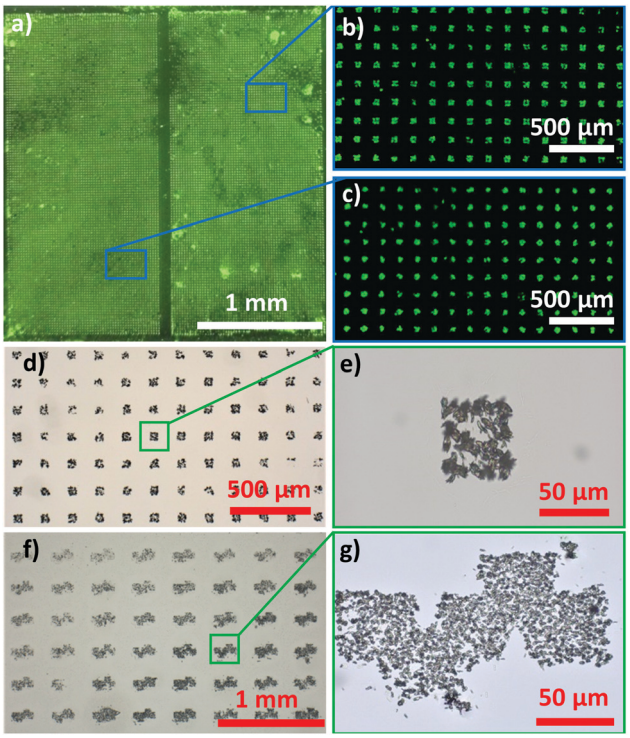

Fig. 3 (a) Photograph of the Tb-MOF pattern on glass under UV light (254 nm); (b and c) magnified patterned regions under UV light (254 nm); (d and e) optical microscopy image of the Tb-MOF in a square pattern and its magnification; (f and g) optical microscopy image of the Tb-MOF in a *TU Graz* Logo pattern and its magnification. All these Tb-MOF patterns were obtained *via* the biomimetic replication of palmitic acid patterns.

biomolecules are ideal candidates for the water-based synthesis of MOF patterns and films.

The authors acknowledge the European Union's Horizon 2020 Programme (FP/2014–2020)/ERC Grant Agreement no. 771834 POPCRYSTAL. The authors thank TU Graz for the Lead Project (LP-03) and Varta Microtechnologies GmbH for the use of SEM.

Conflicts of interest

There are no conflicts to declare.

References

1 P. Falcaro, R. Ricco, C. M. Doherty, K. Liang, A. J. Hill and M. J. Styles, *Chem. Soc. Rev.*, 2014, **43**, 5513–5560.
2 K. Liang, C. Carbonell, M. J. Styles, R. Ricco, J. Cui, J. J. Richardson, D. Maspoch, F. Caruso and P. Falcaro, *Adv. Mater.*, 2015, **27**, 7293–7298.
3 N. K. Maddigan, A. Tarzia, D. M. Huang, C. J. Sumby, S. G. Bell, P. Falcaro and C. J. Doonan, *Chem. Sci.*, 2018, **9**, 4217–4223.
4 E. Astria, M. Thonhofer, R. Ricco, W. Liang, A. Chemelli, A. Tarzia, K. Alt, C. E. Hagemeyer, J. Rattenberger, H. Schroettner, T. Wrodnigg, H. Amenitsch, D. M. Huang, C. J. Doonan and P. Falcaro, *Mater. Horiz.*, 2019, **6**, 969–977.
5 S. Li, M. Dharmarwardana, R. P. Welch, C. E. Benjamin, A. M. Shamir, S. O. Nielsen and J. J. Gassensmith, *ACS Appl. Mater. Interfaces*, 2018, **10**, 18161–18169.
6 R. de Jong and M. de Puit, *Forensic Sci. Int.*, 2018, **291**, 12–16.
7 S. Moret, E. Scott, A. Barone, K. Liang, C. Lennard, C. Roux and X. Spindler, *Forensic Sci. Int.*, 2018, **291**, 83–93.
8 J. Zhuang, A. P. Young and C.-K. Tsung, *Small*, 2017, **13**, 1700880.
9 F. Nudelman and N. A. J. M. Sommerdijk, *Angew. Chem., Int. Ed.*, 2012, **51**, 6582–6596.
10 K. Liang, R. Ricco, C. M. Doherty, M. J. Styles and P. Falcaro, *CrystEngComm*, 2016, **18**, 4264–4267.
11 C. Doonan, R. Riccò, K. Liang, D. Bradshaw and P. Falcaro, *Acc. Chem. Res.*, 2017, **50**, 1423–1432.
12 A. Poddar, J. J. Conesa, K. Liang, S. Dhakal, P. Reineck, G. Bryant, E. Pereiro, R. Ricco, H. Amenitsch, C. Doonan, X. Mulet, C. M. Doherty, P. Falcaro and R. Shukla, *Small*, 2019, 1902268.
13 P. Falcaro, A. J. Hill, K. M. Nairn, J. Jasieniak, J. I. Mardel, T. J. Bastow, S. C. Mayo, M. Gimona, D. Gomez, H. J. Whitfield, R. Riccò, A. Patelli, B. Marmiroli, H. Amenitsch, T. Colson, L. Villanova and D. Buso, *Nat. Commun.*, 2011, **2**, 237.
14 L. S. Ferguson, F. Wulfert, R. Wolstenholme, J. M. Fonville, M. R. Clench, V. A. Carolan and S. Francese, *Analyst*, 2012, **137**, 4686.
15 Y. Nunome, T. Tsuda and K. Kitagawa, *Anal. Sci.*, 2010, **26**, 917–919.
16 A. Girod, R. Ramotowski and C. Weyermann, *Forensic Sci. Int.*, 2012, **223**, 10–24.
17 K. M. Antoine, S. Mortazavi, A. D. Miller and L. M. Miller, *J. Forensic Sci.*, 2010, **55**, 513–518.
18 D. K. Williams, C. J. Brown and J. Bruker, *Forensic Sci. Int.*, 2011, **206**, 161–165.
19 A. Girod and C. Weyermann, *Forensic Sci. Int.*, 2014, **238**, 68–82.
20 S. Oonk, T. Schuurmans, M. Pabst, L. C. P. M. de Smet and M. de Puit, *Sci. Rep.*, 2018, **8**, 16425.
21 M. M. Houck, *Forensic Fingerprints*, Elsevier Science, San Diego, 2016.
22 S. M. Bleay, R. S. Croxton and M. D. Puit, *Fingerprint development techniques: theory and application*, 2018.
23 K. Liang, R. Ricco, C. M. Doherty, M. J. Styles, S. Bell, N. Kirby, S. Mudie, D. Haylock, A. J. Hill, C. J. Doonan and P. Falcaro, *Nat. Commun.*, 2015, **6**, 7240.
24 S. Cadd, M. Islam, P. Manson and S. Bleay, *Sci. Justice*, 2015, **55**, 219–238.
25 S. Hong, I. Hong, A. Han, J. Y. Seo and J. Namgung, *Forensic Sci. Int.*, 2015, **257**, 403–408.
26 P. Innocenzi, L. Malfatti and P. Falcaro, *Water droplets to nanotechnology: a journey through self-assembly*, RSC Publ., Royal Soc. of Chemistry, Cambridge, 2013.
27 C. Nick Pace, S. Treviño, E. Prabhakaran and J. Martin Scholtz, *Philos. Trans. R. Soc. London, Ser. B*, 2004, **359**, 1225–1235.
28 T. M. Reineke, M. Eddaoudi, M. Fehr, D. Kelley and O. M. Yaghi, *J. Am. Chem. Soc.*, 1999, **121**, 1651–1657.
29 C. Daiguebonne, N. Kerbellec, O. Guillou, J.-C. Bünzli, F. Gumy, L. Catala, T. Mallah, N. Audebrand, Y. Gérault, K. Bernot and G. Calvez, *Inorg. Chem.*, 2008, **47**, 3700–3708.
30 N. Kerbellec, D. Kustaryono, V. Haquin, M. Etienne, C. Daiguebonne and O. Guillou, *Inorg. Chem.*, 2009, **48**, 2837–2843.
31 F. F. de Sousa, C. E. S. Nogueira, P. T. C. Freire, S. G. C. Moreira, A. M. R. Teixeira, A. S. de Menezes, J. Mendes Filho and G. D. Saraiva, *Spectrochim. Acta, Part A*, 2016, **161**, 162–169.
32 E. Moreno, R. Cordobilla, T. Calvet, F. J. Lahoz and A. I. Balana, *Acta Crystallogr., Sect. C: Cryst. Struct. Commun.*, 2006, **62**, o129–o131.
33 H. Li, W. Bu, W. Qi and L. Wu, *J. Phys. Chem. B*, 2005, **109**, 21669–21676.
34 O. Shekhah, *Materials*, 2010, **3**, 1302–1315.
35 A.-W. Xu, Y. Ma and H. Cölfen, *J. Mater. Chem.*, 2007, **17**, 415–449.
36 C. Thibault, V. Le Berre, S. Casimirius, E. Trévisiol, J. François and C. Vieu, *J. Nanobiotechnol.*, 2005, **3**, 7.
37 S. Alom Ruiz and C. S. Chen, *Soft Matter*, 2007, **3**, 168–177.